

Ultra-High Energy Cosmic Ray Propagation in the Local Supercluster

Günter Sigl

Department of Astronomy & Astrophysics, The University of Chicago, Chicago, IL 60637-1433

Martin Lemoine

DARC, UPR-176, CNRS, Observatoire de Paris, 92195 Meudon Cédex, France

Peter Biermann

Max-Planck Institute for Radioastronomy, D-53010 Bonn, Germany

(October 15, 2018)

We present detailed numerical simulations and analytical approximations of the propagation of nucleons above 10^{19} eV in the Local Supercluster, assuming that the ambient magnetic field is turbulent, and its strength $0.01 \mu\text{G} \lesssim B_{\text{rms}} \lesssim 1 \mu\text{G}$. In such strong magnetic fields, protons in the low energy part of the spectrum, 10^{19} eV $\lesssim E \lesssim E_C$ diffuse, while the higher energy particles, with $E \gtrsim E_C$ propagate along nearly straight lines. The magnitude of the transition energy E_C depends mainly on the strength of the magnetic field, the coherence length, and the distance to the source; for $B_{\text{rms}} \simeq 0.1 \mu\text{G}$, a largest eddy of length ~ 10 Mpc, and a distance to the source ~ 10 Mpc, $E_C \simeq 100$ EeV. Our numerical treatment substantially improves on previous analytical approximations, as it allows to treat carefully the transition between the two propagation regimes, as well as the effects due to inhomogeneities expected on scales of a few Mpc. We show that a turbulent magnetic field $B_{\text{rms}} \sim 0.1 \mu\text{G}$, close to equipartition, would allow to reproduce exactly the observed spectrum of ultra high energy cosmic rays, up to the highest energy observed, for a distance to the source $d \lesssim 10$ Mpc, for the geometry of the Local Supercluster, *i.e.* a sheet of thickness $\simeq 10$ Mpc. Diffusion, in this case, allows to reproduce the high flux beyond the Greisen Zatsepin Kuzmin cut-off, with a soft injection spectrum $j(E) \propto E^{-2.4}$. Moreover, the large deflection angles at the highest energies observed, typically $\sim 10^\circ$ for the above values, would explain why no close-by astrophysical counterpart could be associated with these events.

PACS numbers: 98.70.Sa, 98.62.En

Keywords: Ultra-high energy cosmic rays, cosmic magnetic fields

I. INTRODUCTION

The structure and strength of extragalactic magnetic fields are very poorly known at present. These fields likely consist of two components: A large-scale component that permeates the whole universe and constitutes a primordial relic of physical processes in the early universe, and a more localized component which is associated with the structure of galaxies, galaxy clusters, and superclusters. For the primordial field only upper limits are known, most notably from the limits on the Faraday rotation of radio waves from distant powerful radio sources [1,4]. For a field of r.m.s. strength B_{rms} and coherence length λ_c , this constraint is $B_{\text{rms}}\lambda_c^{1/2} \lesssim 10^{-9}$ G Mpc $^{1/2}$. For the component of the field that is uniform on the Hubble scale, this constraint reads $B_c \lesssim 10^{-11}$ G. Theoretical scenarios for the origin of this primordial component, *e.g.*, as relic fields produced by the electric currents present during the electroweak or the QCD phase transition [2], or by the Biermann battery effect [3], predict much smaller field strengths, typically of the order of 10^{-20} G. In contrast, positive detections from measurements of Faraday rotation and synchrotron emission exist for the localized component [1,4]. Estimates range from 10^{-9} G up to 10^{-7} G over scales of Mpc, and in some cases up to 10^{-6} G, *e.g.*, in the core of galaxy clusters [1]. Notably, a broad $\sim 50^\circ$ region centered on the Local Virgo Supercluster seems to be endowed with a magnetic field with a uniform component of strength $\sim 1.5 \times 10^{-6}$ G [5], and a random component of strength $\sim 10^{-6}$ G [6]. The coherence length of random components is usually taken to be a cell size of ~ 20 kpc [7].

The origin of this component is unclear, the most common explanations being the action of a dynamo that exponentially amplifies seed fields of the order of 10^{-20} G in the flows of the large scale galaxy structures, adiabatic compression of strong primordial fields in the range $10^{-12} - 10^{-9}$ G, or ejection from radiogalaxies [8] or normal galaxies [9].

After several generations of experiments, most notably the Haverah Park [10], the Akeno Giant Air Shower Array (AGASA) [11,12], and the Fly's Eye [13] experiments, the origin and the nature of ultra high energy cosmic rays (UHE CRs), with energies $E \gtrsim 10$ EeV ($1 \text{ EeV} = 10^{18}$ eV) constitute an unsolved problem as well. Nucleons above a few tens of EeV are limited in their range to at most $\simeq 50$ Mpc, due to the production of pions on the cosmic microwave

background (CMB), known as the Greisen-Zatsepin-Kuzmin (GZK) effect [14]. No compelling astrophysical candidate for the source of the highest energy events could be found within this distance scale [15–17]. Other primaries such as nuclei, γ -rays, or neutrinos, pose similar problems [18]. Theoretical scenarios for their origin include powerful radio galaxies [19], cosmological γ -ray bursts [20], and topological defects left over from phase transitions in the early universe that took place at temperatures near Grand Unification Scales [21,22].

Magnetic fields above $\sim 10^{-12}$ G on Mpc scales significantly influence the propagation of charged cosmic rays up to the highest energies ever observed, namely several 100 EeV, by deflecting and delaying them relative to straight line propagation with the speed of light. The absence of a significant correlation of their arrival directions with the Galactic plane [23] and the fact that protons at these energies cannot be confined within the Galactic magnetic field, suggest that UHE CRs above ~ 1 EeV most likely have their origin in extragalactic sources.

We recently developed a Monte Carlo code for the propagation of nucleons in extragalactic magnetic fields. We demonstrated that a combination of this code with a maximum likelihood approach allows to extract from observed distributions of arrival directions, times, and energies information on the nature of the source mechanism as well as on the strength and structure of large-scale cosmic magnetic fields, without taking recourse to any specific scenario for the origin of UHE CR [24,25]. This was discussed in a qualitative way in Refs. [26,27] and applied to the pairs of events recently reported by the AGASA experiment [12] in Ref. [28]. Our studies were motivated by the fact that future large scale experiments [29], such as the High Resolution Fly’s Eye [30], the Telescope Array [31], and most notably the Pierre Auger project [32], should allow to detect clusters of $\gtrsim 20$, and possibly more, UHE CRs per source, if the clustering suggested by the AGASA results [12] is a real effect caused by discrete sources. The recently proposed satellite observatory concept for an Orbital Wide-angle Light collector (OWL) [33] might even allow to detect clusters of hundreds of events by watching the Earth’s atmosphere from space.

In our studies we adopted a statistical description of the extra-galactic magnetic field as a Gaussian random field in Fourier space with zero mean and a power spectrum with $\langle B^2(k) \rangle \propto k^{n_B}$ for $k < 2\pi/l_c$ and $\langle B^2(k) \rangle = 0$ otherwise, where l_c is the numerical cut-off scale. Our studies were thus performed for a “homogeneous” magnetic field, and, furthermore, assuming near straight line propagation, *i.e.* $B_{\text{rms}} \lesssim 10^{-9}$ G. The subject of the present work is to generalize this to the case of more complex structures of cosmic magnetic fields, most notably the possibility of a locally enhanced magnetic field associated with the Local Supercluster. Indeed, Ryu, Kang & Biermann [34] have recently argued that the upper limit on the strength of a homogeneous magnetic field, obtained from Faraday rotation measures of distant quasars, becomes $B \lesssim 1\mu\text{G}$ in filaments and walls of large scale structure, under the very reasonable assumption that the magnetic field scales with the matter density. On the other hand, if the two paired events observed by AGASA close to the Supergalactic plane are due to discrete sources and not a statistical fluctuation, the field strengths in this structure must be smaller than $\sim 10^{-9}$ G. However, Biermann et al. [35] have argued that due to the accretion flow with embedded magnetic fields towards the Supergalactic plane, weak confinement is possible, in which case the AGASA pairs could have originated in unrelated sources. The existence of strong magnetic fields in the local Supercluster is therefore an unsettled issue.

Particles above ~ 10 EeV, that propagate over cosmological distances in magnetic fields as strong as $B \gtrsim \text{few} \times 10^{-8}$ G, enter the diffusion regime in which they turn around several times before reaching the observer. However, above a certain energy E_C , whose value depends on the strength of the magnetic field, on the coherence length, and on the distance to the source, charged UHE nucleons do not diffuse, and rather propagate in a near straight line. This scenario, proposed by Wdowczyk & Wolfendale [36], has several attractive features with respect to the observed UHE CR spectrum. The transition between diffusion and near straight line propagation could *a priori* explain why the UHE CR spectrum appears flatter above ~ 100 EeV than below, although this trend is not confirmed due to a lack of statistics at high energy. Moreover, such strong magnetic fields would result in large deflection angles, even at the highest energies observed, and would thus explain why no astrophysical counterpart could be associated with these events. Finally, the work of Ryu, Kang & Biermann [34] seems to support the idea that the magnetic field could be much stronger within walls and filaments of large scale structure, than in the voids. The spectra of UHE CRs in such structures have to some extent been discussed for the diffusive limit in Ref. [37].

Recently, the diffusion of UHE CRs in the local supercluster has been reconsidered in Ref. [38]. These authors combined the diffusion approximation at low energies with the straight line propagation approximation at high energies, assuming continuous energy losses and an infinitely thick supergalactic plane. The main difference to Ref. [36] lies in a better treatment of energy losses, a more careful treatment of the transition regime between diffusion and rectilinear propagation, a more quantitative appraisal of the diffusion coefficient, and a more detailed discussion with respect to present data. One goal of the present work is to overcome the approximations made in Refs. [36,38], *i.e.* to provide more accurate flux calculations at “intermediate” energies where both the diffusion and the small deflection approximations break down, and to examine the effect of an inhomogeneous distribution of densities and magnetic fields in the local Supercluster. This latter effect is especially important as the distance to the nearest cluster (Virgo, $d \sim 20\text{Mpc}$) is already larger than the typical scale of these inhomogeneities for which a few Mpc is a reasonable assumption.

We describe our approach in Section 2, present results of the numerical simulations in Section 3, and conclude in Section 4. Natural units are used throughout, i.e., $c = \hbar = 1$.

II. NUMERICAL APPROACH

A detailed account of our approach was given in Refs. [28,24]. Here, we restrict ourselves to a brief description of the most important aspects and the generalizations relevant for the present study.

A specific scenario is characterized by the magnetic field realization and the position of source and observer. For each such scenario, we computed a few 10^3 trajectories of nucleons emitted from a given source in random directions within a cone with opening angle of typically 90° and with a flat injection spectrum. This was done by solving the equations of motion in the presence of the magnetic fields, taking into account pion production losses by sampling the relevant differential cross sections, as well as losses from pair production by protons on the CMB as a continuous energy loss process. If the nucleon crossed the sphere of radius d around the source on a cap with an opening angle of typically a few degrees, centered on the observer, the nucleon was considered as arriving to the observer. In this case its injection energy, and the energy, time, and propagation direction upon arrival, the latter defined relative to the line of sight to the source, were recorded. The trajectory of the nucleon does not stop here, however, as, in the diffusion regime, one needs to calculate the number density of particles at a given point. Therefore, in our calculations, a given nucleon propagates until either the propagation time exceeded 10^{10} yr, or the distance exceeded twice the distance d between the source and the observer, and, on its way, it can give multiple hits on the “detector”. Since particles crossing the cap from either side were considered as arriving, the maximal deflection angle is 180° . The contribution of a particular particle to the flux per area is weighted by the inverse of the absolute value of the cosine of the arrival direction relative to the line of sight to the source. If the linear dimension of the cap centered at the observer is comparable or smaller than the typical gyro radius of the particle and the coherence length of the magnetic field, and the emission cone angle is larger than typical deflection angles, this procedure ensures a realistic distribution of arrival energies, times, and directions without too excessive use of CPU time. By varying the cone angles within these limits, we verified the independence of the results of the exact cone angle values. Our procedure applies to arbitrary magnetic field strengths and deflection angles.

The resulting distributions of UHE CRs can be folded with the source emission timescale T_S in time and with the injection spectrum in energy to obtain distributions for arbitrary T_S and injection spectra. Since we consider turbulent magnetic fields, defined by a Kolmogorov spectrum, the spatial configuration of the magnetic field is highly anisotropic, as seen from, either the source, or the observer. We thus perform ~ 10 runs for a given set of parameters, in order to circumvent, and, at the same, examine, the effect of a particular realization of the field on the spectrum.

We approximate the structure of the local Supercluster as an infinitely extended two-dimensional sheet of half-thickness d_s in the $x - y$ plane at a position z_s . For the density profile $\rho(z)$ we assumed a Gaussian of the form

$$f(z) \equiv \rho(z)/\rho_0 = \left\{ \frac{1}{c} + \exp \left[- \left(\frac{z - z_s}{d_s} \right)^2 \right] \right\}, \quad (1)$$

where c is the density contrast and ρ_0 is the density at the center of the sheet. It is possible to include a further radial dependence of the density profile; however, for the sake of simplicity, we will ignore such dependence in the following and take the sheet to be uniform in the $x - y$ plane.

The random component of the magnetic field is then modeled by using the Fourier transformed Gaussian field of strength B_{rms} with the power law spectrum described earlier, truncated below $k_{\text{min}} = 2\pi/L$, with L the largest turbulent eddy, and above $k_{\text{max}} = 2\pi/l_c$, and multiplying it with the profile $f(z)$. This does not strictly speaking obey $\nabla \cdot \mathbf{B} = 0$, but we do not expect this to significantly influence the calculated histograms. For the power law index we choose $n_B = -11/3$, corresponding to a turbulent Kolomogov spectrum.

In addition, the continuity equation and Maxwell’s equations allow for a coherent field component B_c that is parallel to the sheet and whose only dependence is on z and is proportional to $f(z)$. We have verified in our Monte Carlo simulations that a coherent component of strength considerably smaller than the random component does not change results significantly. For this reason we will neglect a coherent component altogether in the rest of this paper.

Strictly speaking, due to the high conductivity of the extragalactic medium, the accretion flow onto the sheet causes an electric field $\mathbf{E} = -\mathbf{v} \times \mathbf{B}$, where \mathbf{v} is the velocity field. Because $v \ll 1$, we will, however, neglect this field in the present simulations. Other interactions, such as with baryons, are also negligible. We note, however, that solar modulation of cosmic rays depends on this electric field, which thus may be necessary to include in future studies.

In our simulations we usually consider one discrete source located at the origin of the coordinate system, and the observer location is characterized by its z coordinate z_o , and its distance d to the source; the source itself is

characterized by a z coordinate z_s . In order to reduce the parameter space, we assume, in all simulations, a sheet thickness $d_s = 5$ Mpc, a largest turbulent eddy of size $L \sim 2d_s$, and a magnetic field cut-off scale $l_c = L/10$. The latter is limited by resolution but does not influence the result as long as $l_c \ll L$ because the magnetic field power is concentrated at the largest scales. For this reason, the effective coherence scale of magnetic fields with a Kolomogorov spectrum is given by $\lambda_c \simeq L/(2\pi)$. We further assume power law differential injection spectra $Q(E) \propto E^{-\gamma}$, extending up to $E = E_{\max} = 10^4$ EeV, but we note that because of the falling fluxes the results and conclusions are independent of maximal energies E_{\max} for $E_{\max} \gtrsim 10^3$ EeV.

III. RESULTS

Here, unless otherwise stated, we assume a stationary situation, *i.e.* such that the emission timescale of the source is much longer than the diffusion timescale (typically $\sim 10^8$ yr). Sources with smaller emission time scales tend to produce spectra that are peaked at specific energies, and, therefore, individually provide much poorer fits to the combined data above ~ 10 EeV.

A. Diffusion of UHE CRs in an infinite medium

We first recall the effect of diffusion in an infinite medium on charged UHE CRs. A similar discussion of this topic is given in Ref. [38]. Ignoring energy losses for a moment, there will be a transition energy E_C such that particles with $E \gg E_C$ will propagate along nearly straight lines, whereas particles with $E \ll E_C$ will diffuse. This transition occurs where the (energy-dependent) time delay τ_E with respect to rectilinear propagation with the speed of light becomes comparable to the distance d . Since in the rectilinear regime, $E \gtrsim E_C$, the time delay is given by

$$\tau_E \simeq \frac{2}{5} \frac{d^2 L}{18 r_g^2} \simeq 6 \times 10^3 \left(\frac{E}{100 \text{ EeV}} \right)^{-2} \left(\frac{d}{10 \text{ Mpc}} \right)^2 \left(\frac{L}{10 \text{ Mpc}} \right) \left(\frac{B_{\text{rms}}}{10^{-9} \text{ G}} \right)^2 \text{ yr}, \quad (2)$$

assuming $n_B = -11/3$, where $r_g = E/(eB_{\text{rms}})$ is the gyro radius (e is the electron charge), this condition translates into

$$E_C \simeq 150 \left(\frac{d}{10 \text{ Mpc}} \right)^{1/2} \left(\frac{B_{\text{rms}}}{10^{-7} \text{ G}} \right) \left(\frac{L}{10 \text{ Mpc}} \right)^{1/2} \text{ EeV}. \quad (3)$$

This estimate is confirmed by our numerical simulations within a factor of about 2, for our parameters chosen. For $E \gtrsim E_C$, the observable differential spectrum per solid angle (current density) $j(E)$ is unmodified by the magnetic field with respect to the injection spectrum and given by

$$j(E) = \frac{Q(E)}{(4\pi)^2 d^2}. \quad (4)$$

The diffusive regime, $E \lesssim E_C$, is usually described by an energy-dependent diffusion coefficient $D(E)$, and the expressions corresponding to Eqs.(2) and (4) read

$$\tau_E \simeq \frac{d^2}{D(E)}, \quad (5)$$

and

$$j(E) = \frac{Q(E)}{(4\pi)^2 d D(E)}, \quad (6)$$

respectively.

Another way of defining the transition energy E_C is to equate Eqs. (4) and (6) which gives $d = D(E_C)$. For the Bohm diffusion coefficient $D_{\text{Bohm}}(E) = r_g/3$, this results in $E_C \simeq 3.3 \times 10^3 (d/10 \text{ Mpc}) (B_{\text{rms}}/10^{-7} \text{ G})$ EeV, about a factor 20 higher than Eq. (3) for our parameters. These estimates suggest that the transition regime between the analytically tractable limiting cases of diffusion and rectilinear propagation may stretch more than one order of magnitude in energy and further emphasizes the need for detailed numerical simulations in that regime.

For a diffusion coefficient that scales as $D(E) \propto E^m$, one thus obtains $j(E) \propto E^{-\gamma-m}$, in the absence of energy losses. From the approximate analytical expression

$$D(E) \simeq \frac{1}{3} r_g(E) \frac{B_{\text{rms}}}{\int_{1/r_g(E)}^{\infty} dk k^2 \langle B^2(k) \rangle}, \quad (7)$$

where $B_{\text{rms}}^2 = \int_0^{\infty} dk k^2 \langle B^2(k) \rangle$, one expects $m \sim 1$ for $r_g \gtrsim L/(2\pi)$ from Bohm diffusion, and $m \sim 1/3$ for $r_g \lesssim L/(2\pi)$ in the case of the Kolmogorov spectrum. As a consequence, the correlation between the time delay τ_E and E should switch from, roughly, $\tau \propto E^{-1/3}$ at largest time delays, hence smallest energies, as long as $r_g \lesssim L/(2\pi)$, to $\tau_E \propto E^{-1}$ in the regime of Bohm diffusion, $r_g \gtrsim L/(2\pi)$, and eventually to $\tau \propto E^{-2}$ at the smallest time delays, hence largest energies, in the near straight line propagation regime, $E \gtrsim E_C$. As we discuss below, our simulations indeed show all three propagation regimes, up to the difference that the diffusing regime with $D(E) \propto E^{1/3}$ takes place when $r_g < 0.1L/(2\pi)$, and $D(E) \propto E$ otherwise as long as diffusion holds.

The above picture is easily derived from analytical calculations. However, such calculations cannot reproduce very well the transition between the diffusive regime and the regime in which particles propagate nearly linearly. In Figure 1, we show, as the thin solid histogram, the spectrum obtained for UHE CRs propagating in a $B_{\text{rms}} \simeq 5 \times 10^{-8}$ G magnetic field, over a distance $d = 10$ Mpc, in an infinite medium, in the absence of energy losses, and for an injection spectrum $\propto E^{-2}$. In the low energy region, $10 \text{ EeV} \lesssim E \lesssim 70 \text{ EeV}$, where Bohm diffusion occurs, one recovers the slope predicted by Eq. (6), $j(E) \propto E^{-2}/D(E) \propto E^{-3}$. At high energy, $E \gtrsim 100 \text{ EeV}$, where particles propagate in near straight line, one recovers the injection spectrum, *i.e.*, the spectrum is not modified during propagation. The transition between the two regimes indeed occurs smoothly, as would be obtained from a simple interpolation. Our simulations allow us to derive the magnitude of the diffusion by equating the ratio of numerical fluxes in the diffusive and rectilinear regimes with the ratio of Eqs. (6) and (4). It is thus not set *a priori*; we obtain, for this latter: $D(E) \simeq 3 \times 10^{32} \text{ cm}^2 \text{ s}^{-1} (E/1 \text{ EeV})(B_{\text{rms}}/1 \mu\text{G})^{-1}$, *i.e.* a factor $\simeq 10$ higher than the Bohm diffusion coefficient. This is consistent with the above mentioned fact that we observe Bohm diffusion for $r_g > 0.1L/(2\pi)$ and suggests that the magnetic field structure in the numerical simulation leads to an effective gyro radius that is about a factor 10 higher than the analytical expression $r_g = E/(eB_{\text{rms}})$.

We now turn to the effects caused by energy losses. Their overall effect in the Monte Carlo simulations is shown in Figure 1 as the thick solid histogram, for the same physical parameters as above. The qualitative effect of the introduction of pion production and pair production losses, for $d \simeq 10$ Mpc, is to change the slope to roughly $j(E) \propto E^{-2.6}$ ($\gamma = 2$), and to deplete the flux at high energies, in favor of the flux at low energies, as pion production occurs mainly above the GZK cut-off at $\sim 50 \text{ EeV}$.

Analytically, energy losses are often approximated as being continuous, in which case the rate of change of the particle energy is governed by the equation $dE/dt = b(E)$. We note that this is not necessarily a good approximation because the dominant energy loss process, namely pion production, is purely stochastic and not continuous. Our Monte Carlo simulations do not make this approximation.

An often used analytical expression for the flux from a point source at distance d in the rectilinear regime [39] which generalizes Eq. (4) is then given by (we neglect redshifting)

$$j(E) = \frac{Q[E_i(E, d)]}{(4\pi)^2 d^2} \frac{dE_i(E, d)}{dE}, \quad (8)$$

where $E_i(E, r)$ satisfies the equation $\partial_r E_i(E, r) = -b[E_i(E, r)]$ with $E_i(E, d) = E$; $dE_i(E, d)/dE$ is the ratio of energy intervals at emission and observation.

In the diffusive regime the problem can be described by a partial differential equation for the local density $n(E, \mathbf{r}) = 4\pi j(E, \mathbf{r})$ of UHE CRs of the following form

$$\partial_t n(E, \mathbf{r}) + \partial_E [b(E)n(E, \mathbf{r})] - \nabla [D(E)\nabla n(E, \mathbf{r})] = q(E, \mathbf{r}), \quad (9)$$

where $q(E, \mathbf{r})$ is now the differential injection rate per volume, $Q(E) = \int d^3\mathbf{r} q(E, \mathbf{r})$. Eq. (9) also holds if $D(E)$ is space dependent (see next section). In the homogeneous case, an analytical solution of Eq. (9) is known [40] which for a point source can be written as

$$j(E) = \frac{1}{4\pi} \int_0^{+\infty} dE' \frac{Q(E')}{|b(E)|(4\pi\lambda^2)^{3/2}} \exp\left[-\frac{d^2}{4\lambda(E, E')^2}\right], \quad (10)$$

where

$$\lambda(E_1, E_2) \equiv \left[\int_{E_2}^{E_1} dE' \frac{D(E')}{|b(E')|} \right]^{1/2}, \quad (11)$$

denotes an effective path length against losses [$\lambda(E_1, E_2) \equiv 0$ if $E_1 > E_2$].

In the simplest approximation, Eq. (8) and analytical solutions of Eq. (9) are just used for $E > E_C$ and $E < E_C$, respectively [36,38]. For the diffusive solution, the above integral should then be truncated at E_C . A somewhat better analytical approximation can actually be obtained by treating particles as propagating rectilinearly as long as $E > E_C$ *in flight*, but diffusively otherwise. For a point source, this amounts to adding in “secondary sources” in Eq. (9), corresponding to the spatial distribution of high energy particles, with $E > E_C$ at injection, that have propagated rectilinearly and lost energy down to E_C . The source term is thus replaced by:

$$q(E, \mathbf{r}) \longrightarrow q(E, \mathbf{r})\Theta(E_C - E) + \int d^3\mathbf{r}_i \frac{q[E_i(E_C, |\mathbf{r} - \mathbf{r}_i|), \mathbf{r}_i]}{4\pi|\mathbf{r} - \mathbf{r}_i|^2} \frac{dE_i(E_C, |\mathbf{r} - \mathbf{r}_i|)}{dE} |b(E_C)|\delta(E - E_C) \quad (12)$$

on the r.h.s. of Eq. (9), where $\Theta(x)$ is the Heaviside function, \mathbf{r}_i denotes the “secondary” source location; for a point-like source, $q(E, \mathbf{r}) = Q(E)\delta^3(\mathbf{r} - \mathbf{r}_s)$. This changes the flux towards higher values if E_C is larger than the GZK cutoff ~ 50 EeV.

We show the analytical predictions Eqs. (6) and (4) (in the absence of energy losses), and Eqs (9), (12), and (8) (including energy losses) as light and thick solid lines respectively, in Fig. 1, for comparison with the Monte Carlo results. The continuous energy loss rate $b(E)$ was taken from Refs. [39,41]. The diffusion coefficient that enters the analytical solution of the diffusion equation has been normalized to the value obtained from the numerical solutions for a homogeneous medium in the absence of energy losses. We note that the analytical solution, when energy losses are included, does not reproduce correctly the transition between the two different propagation regimes. As would be naively expected, the energy losses around the GZK cut-off tend to smooth out the spectrum in this transition region. Up to this inadequacy of the sudden transition approximation, and the difference in energy losses (obvious at high energy), there is good agreement between the two methods, in this standard case.

B. Diffusion of UHE CRs in the Local Supercluster

When diffusion occurs in a sheet of finite thickness, the above picture is significantly modified. For a better comprehension of the different physical effects that enter the discussion, we distinguish here two different regimes: one in which the diffusive regime takes place only for particles with energy less than the GZK threshold $\simeq 50$ EeV, and the other in which particles with energies greater than the GZK cut-off also diffuse. For a distance $d \simeq 10$ Mpc, and the above choice of parameters, these two regimes roughly correspond respectively to $B_{\text{rms}} \lesssim 5 \times 10^{-8}$ G, and $B_{\text{rms}} \gtrsim 10^{-7}$ G.

We first discuss the case where diffusion occurs only below the GZK cut-off. Since the observed UHE CR spectrum between ~ 5 EeV up to the GZK cut-off can be fit with one power law, we select $B_{\text{rms}} \simeq 5 \times 10^{-8}$ G as a fiducial value, in which case particles up to the GZK cut-off diffuse, for a source distance $d \sim 10$ Mpc. The main effect due to the finite thickness of the sheet is that particles can escape freely at the boundary of the sheet, since the magnetic field outside is too weak to turn the particles around. Therefore, the energy spectrum of UHE CRs is depleted in the energy range where particles diffuse, whenever the source and/or the observer are located near the boundary, or when the distance to the source is much larger than the sheet thickness. It is important to note that this effect occurs only for those particles that diffuse, as the high energy particles that travel in near-straight line are not affected by the presence of the boundary. We recall that diffusion of UHE CRs in the local Supercluster was precisely suggested as a mechanism to enhance the local density of low energy particles, with respect to that of high energy particles. We thus see that the free escape of UHE CRs at the sheet boundary tends to cancel this enhancement.

This main effect is shown as the thin solid histogram in Fig. 2, for a source distance $d = 10$ Mpc, a sheet half-thickness $d_s = 5$ Mpc, an injection $\propto E^{-2}$, other physical parameters as above, and no energy losses taken into account. The same case with energy losses included is shown as the thick solid histogram. The direct comparison of this figure with Fig. 1, in the absence of energy loss, shows that the flux of particles that diffuse in the sheet, is depleted by a factor $\simeq 5$, with respect to the flux of particles diffusing in an infinite medium.

The shape of the spectrum is, however, not significantly changed, and still goes as $Q(E)/D(E)$. This is in agreement with the analytical solution for the sheet geometry, assuming $j(E) = 0$ at the sheet boundaries. For a point source this solution which generalizes Eq. (10) can be written as

$$j(E) = \frac{1}{4\pi} \sum_{m=0}^{+\infty} \cos \left[\left(m + \frac{1}{2} \right) \pi \frac{z_o}{d_s} \right] \cos \left[\left(m + \frac{1}{2} \right) \pi \frac{z_s}{d_s} \right] g_m(r_o, r_s), \quad (13)$$

where r_o, z_o, r_s, z_s respectively denote the cylindrical coordinates of the observer and of the source, and $g_m(r_o, r_s)$ is given, in the absence of energy losses, by

$$g_m(r_o, r_s) = \frac{Q(E)}{2\pi d_s D(E)} K_0 \left[\left(m + \frac{1}{2} \right) \pi \frac{|r_o - r_s|}{d_s} \right], \quad (14)$$

where K_0 is a modified Bessel function of order 0, and, when energy losses are included:

$$g_m(r_o, r_s, E) = \int_0^{+\infty} dE' \frac{Q(E')}{|b(E)| 4\pi \lambda^2 d_s} \exp \left[- \left(m + \frac{1}{2} \right)^2 \pi^2 \frac{\lambda(E, E')^2}{d_s^2} \right] \exp \left[- \frac{(r_o - r_s)^2}{4\lambda(E, E')^2} \right]. \quad (15)$$

These analytical solutions are shown in Fig. 2 as light and thick solid lines, respectively. In this figure, the solution that takes energy losses into account does not mix the two populations of particles, $E > E_C$ and $E < E_C$, *i.e.*, “secondary sources” are not included here, as they were for the infinite medium. However, as numerical solutions of Eqs. (9) and (12) show, inclusion of secondary sources does not change the result significantly in this case where $E_C \lesssim 70$ EeV. We note again that in our simulations, the nucleons are propagated until either the distance traveled is larger than a Hubble time, or twice the distance from the source to the observer. This means that, in practice, the sheet is not infinite, and rather corresponds to a disk, of radius $2d$, and half-thickness d_s . It is possible to obtain analytical solutions corresponding to that case, although such expressions are rather cumbersome [40]. Moreover, the above solution should provide a relatively good approximation, as long as $2d > d_s$, and we are here in this case.

Let us comment briefly on Fig. 2. In this figure, the diffusion coefficient that gives the best fit between the analytical solution and the Monte-Carlo is a factor $\simeq 8$ higher than the Bohm diffusion coefficient, to be compared with a factor $\simeq 10$ in the previous case (Fig. 1) of the infinite homogeneous medium. This slight difference is due to the fact that, in the above analytical solution, the diffusion coefficient is uniform in space, *i.e.* the solution does not take into account the profile of the magnetic field in the sheet. The diffusion coefficient, as averaged over the thickness, is then $\simeq 1.25$ times larger than the corresponding uniform diffusion coefficient, for the same magnetic field strength in the middle plane of the sheet. In the infinite homogeneous case, there is no such profile, and the above factor compensates for the difference between the diffusion coefficients. We also note, in Fig. 2, that the transition between the diffusive and rectilinear regimes does not appear to proceed smoothly. There is a peak around ~ 200 EeV, which showed up for most spatial realizations of the magnetic field. We discuss further below this dependence of the energy spectrum on the particular realization of the turbulent magnetic field. The comparison of the two cases, with and without energy losses, in Fig. 2, shows that this peak is smoothed out by energy losses, as expected. Thus, when the geometry of the sheet is taken into account, the above simple analytical solutions do not compare as well to the Monte-Carlo simulations, as they did for the homogeneous case.

We wish to stress the importance of the particular geometry of the sheet, as it precisely counteracts the effect of diffusion, in depleting the flux at low energies. Several other effects, which we now discuss, add up to this.

The profile of the magnetic field in the sheet is such that the field is stronger in the middle plane than on the boundaries of the sheet. Therefore, if source and observer are located on opposite sides of the middle plane, diffusive low energy particles are here as well depleted with respect to non-diffusive high energy particles. This effect is not important as long as source and observer are located within $\pm d_s/2$ of the middle-plane, and, outside of this range, is dominated by the above effect of free escape due to the proximity to the boundary. Therefore, we do not discuss it further.

In the presence of a sheet, the geometry of the problem becomes highly anisotropic. It is all the more anisotropic when the distance to the source is smaller or comparable to the largest turbulent eddy, *i.e.* $d \lesssim L \sim 10$ Mpc in our case, where most of the power of the magnetic field lies. Indeed, particles of different energies follow different paths, which, depending on the spatial realization of the magnetic field, may, or may not, drive the particles out of the sheet. As far as the UHE CR spectrum is concerned, this effect translates itself in very substantial variations of the flux at a given energy, in the diffusing regime, $\delta j(E)/j(E) \sim 1$. It is important to note that this effect does not represent an overall variation of the flux, but is differential in energy. In Fig. 3, we show two simulations each consisting of 4000 particles in total, obtained from the same parameters as above, that correspond to two different spatial realizations of the magnetic field. These are shown in solid line. We also show the mean flux, as obtained from the average of 13 such simulations, *i.e.* 13 such realizations of the field, in solid histogram. And, we also show the upper and lower 1σ deviations from the mean, which show $\delta j(E)/j(E) \sim 1$. The two particular realizations are not extreme in any respect, and certainly show that the flux is highly dependent on the particular realization of the magnetic field. This strong variation implies that analytical solutions, which solve a diffusion equation that is already spatially averaged over the realizations of the magnetic field, are invalidated as long as they claim to solve a one source – one magnetic field model. In the limit of high energies E , where the influence of the magnetic field is negligible, the scatter $\delta j(E)$ should go to zero. The finite scatter around the mean flux visible in Fig. 3 and the subsequent ones is due to the finite numerical statistics of 4000 particles per field realization.

In the case of an infinite medium, there is also substantial variation of the flux at a given energy; it is not as strong, however, as when a sheet is present, for the reasons given above. Our explanation is further supported by the fact that, for a simulation where the power index of the magnetic field fluctuations is positive, *i.e.*, where the power is concentrated on small scales $\lambda_c \lesssim l_c = 1$ Mpc, the relative deviation of the flux from the mean is not significant.

Qualitatively speaking, if one wishes to reproduce the observed UHE CR spectrum with the help of diffusion in the Local Supercluster, there are several paths to follow. In either case, one has to find a way to increase the flux of UHE CR at the lowest energies $\lesssim 50$ EeV. Therefore, one could select a situation in which $d < d_s$, so that the boundary of the sheet does not play a significant role. The closest energetic galaxy is Centaurus A, at a distance $\simeq 5$ Mpc. In Fig. 4, we show the best fit we were able to obtain for $d = 5$ Mpc, out of 16 spatial realizations of the magnetic field, using an injection spectrum $\propto E^{-2.4}$ in order to match the observations; other physical parameters are as above. All other spatial realizations did not give a satisfying agreement with observations, and, even in this case, the fit is only barely acceptable. However, we certainly cannot exclude all spatial realizations as consistent solutions, in the present case. Our simulations only show that such a solution, if it exists, is *a priori* unlikely, where the *a priori* refers to the statistical distribution of field realizations.

Another way to follow would be, loosely speaking, to increase the energy losses so as to increase the flux at low energies with respect to that at high energies. One should not increase the distance, however, as free escape would then affect the low energy part of the spectrum even more dramatically. This is shown in Fig. 5, where the flux is shown for a source distance $d = 25$ Mpc, all other parameters as above. However, if one increases the strength of the magnetic field, particles with energies higher than the GZK cut-off start to diffuse. Diffusion increases the distance traveled to $d + \tau_E$. Pion production is then affected by the magnetic field as soon as $\tau_E \sim d$, which occurs, for $E \gtrsim 50$ EeV, for $B_{\text{rms}} \gtrsim 10^{-7}$ G, and $d \sim 10$ Mpc, as seen from Eq. (2). Furthermore, a stronger magnetic field results in a smaller diffusion coefficient, which, in turn, implies a higher number density of diffusing particles, all things being equal. Let us now furnish this discussion with more quantitative arguments.

In Fig. 6, we show an extreme case, where $B_{\text{rms}} \simeq 3 \times 10^{-7}$ G, and the injection spectrum $\propto E^{-2.4}$. There, particles up to ~ 200 EeV diffuse, and the effective distance that they travel is $\sim 1.4 \times d \sim 14$ Mpc for $E \sim 100$ EeV, and $\sim 3 \times d$ for $E \sim 70$ EeV, with a large relative scatter in the distance traveled of order 1, at all energies. In this extreme case, pion production is very strong: particles are strongly depleted at high energies due to energy losses, while lower energy particle abundances are increased due to diffusion and energy losses of higher energy particles. Because all three regimes in the correlation between τ_E and E described in the previous section appear in this case above 10 EeV, we show in Fig. 7, the corresponding distribution of UHE CRs in the time delay–energy plane. There one can see the correlation $\tau_E \propto E^{-2}$ at high energies $E \gtrsim 200$ EeV, and the associated scatter, that results from stochastic pion production losses. Below these energies, where particles diffuse, the correlation switches to $\tau_E \propto E^{-1}$ in the Bohm regime, and to $\tau_E \propto E^{-1/3}$ for $E \lesssim 60$ EeV. Note that the gyro radius of a 60 EeV proton in a 3×10^{-7} G magnetic field is $r_g \simeq 200$ kpc $\simeq 0.1L/(2\pi)$. Our simulations thus indicate that the $D(E) \propto E^{1/3}$ correlation only arises when $r_g < 0.1L/(2\pi)$, and $D(E) \propto E$ otherwise. Furthermore, Figs. 6 and 7 indicate that the transition regime between diffusion and rectilinear propagation is rather narrow, a factor 2–3 in energy. This is consistent with the two estimates of the transition energy E_C from Eq. (3) and from $d = D(E_C)$, if the diffusion coefficient derived from the simulations, $D(E) \simeq 10D_{\text{Bohm}}(E)$, is used in the latter.

The best, and consistent, fit to the data is obtained for the intermediate value of the magnetic field strength, $B_{\text{rms}} \simeq 10^{-7}$ G, and an injection spectrum $\propto E^{-2.4}$. Amazingly, this injection spectrum has been derived for UHE CRs from clusters of galaxies [42]. In Fig. 8, we show the resulting UHE CR spectrum, with the associated upper and lower 1σ deviations. Most realizations of the magnetic field give, in this case, acceptable fits to the observed spectrum.

For the sake of illustration, we show in Fig. 9, the angular images at different energies, as indicated, associated with a typical realization corresponding to the case shown in Figs. 2 and 3, but for our standard injection spectrum with $\gamma = 2.4$. Interestingly, a cross-over from several images of the same source at low energies to only one image at the highest energies can be observed. This transition occurs at an energy for which the linear deflection $d\theta_E$ (θ_E being the deflection angle) becomes comparable to the field coherence scale λ_c . This would in turn allow to estimate λ_c . Furthermore, for $E \gtrsim 200$ EeV, the typical deflection angle is $\simeq 13^\circ$. This gives the order of magnitude of the angular box in which one should look for counterparts associated with the highest energy events observed.

Finally, for continuously emitting sources, the source power Q required to reproduce the spectra discussed here is easily estimated as

$$\begin{aligned}
 Q \equiv \int dE Q(E) &= \sim (4\pi)^2 d^2 E^2 j(E) \max \left[(E_{\text{max}}/E)^{(2-\gamma)}, (E_{\text{min}}/E)^{(2-\gamma)} \right] \\
 &\sim 7.2 \times 10^{45} \left(\frac{d}{10 \text{ Mpc}} \right)^2 \max \left[(E_{\text{max}}/E)^{(2-\gamma)}, (E_{\text{min}}/E)^{(2-\gamma)} \right] \text{ erg s}^{-1}
 \end{aligned} \tag{16}$$

at energies E where deflection is small. Here, E_{\min} is the low energy cut-off of the injection spectrum (relevant if $\gamma > 2$), and the second expression has been obtained from the observed flux at $E \simeq 300$ EeV. This model, for a single source, active over $\gtrsim 10^8$ yr, thus requires a very high cosmic ray luminosity, in agreement with previous estimates [36]. For comparison, the observed luminosity of NGC 4151, a powerful Seyfert galaxy of the local Supercluster, located at a distance ~ 13 Mpc (for $H_0 = 75$ km/s/Mpc), is $L \sim 10^{45}$ erg/s, and the typical bolometric luminosity of a Seyfert galaxy is $L \sim 10^{44} - 10^{46}$ erg/s. On the theoretical side, expectations for the UHE CR luminosity are uncertain and vary greatly with the type of accelerator and the emission timescale, *e.g.*, $L_{\text{UHECR}} \sim 10^{46}$ erg/s for acceleration in Active Galactic Nuclei over $\sim 10^8$ yr, $L_{\text{UHECR}} \sim 10^{51}$ erg/s over ~ 100 s for fireball models of γ -ray bursts, up to $L_{\text{UHECR}} \gtrsim 10^{52}$ erg/s over $\gtrsim 1$ s – 10^4 yr (spread in photons, neutrinos, and nucleons), for topological defects, and up to $L_{\text{UHECR}} \sim 3 \times 10^{47}$ erg/s for radiogalaxies [43].

A one source model, such as considered above, certainly demands a huge output of energy in UHE CRs, when one integrates the required luminosity over the required emission timescale. Nevertheless, we note that intermittent sources, with pulses of duration $T \ll \tau_E \sim 10^8$ yr, with inter-pulse durations $\Delta T \ll \tau_E$, and, preferably $T \ll \Delta T$, would mimic a continuously emitting source, as the scatter in time delays $\delta\tau_E \sim \tau_E \gg \Delta T$. Obviously, the energy budget would then be greatly alleviated. In fact, the hot spots in radiogalaxies that are believed to be UHE CR sources [19] show intermittent behavior on time scales of $\sim 10^4$ yr and smaller. Also, nothing prevents us from considering more than one source; for instance, there are at least seven powerful Seyfert galaxies in the Local Supercluster, whose distance lies between ~ 5 Mpc and ~ 20 Mpc. As well, the combination of many bursting sources, with emission timescales $\ll 10^8$ yr, would reproduce a spectrum similar to that of a single continuously emitting source.

Finally, we note that the injection spectrum index that we considered here, $\gamma = 2.4$, is very close to the value expected from acceleration in ultra-relativistic shocks $\simeq 2.2 \pm 0.1$ [44].

IV. CONCLUSIONS

We have discussed the propagation of charged UHE CR nucleons in a locally enhanced extra-galactic magnetic field of strength $B_{\text{rms}} \gtrsim 10^{-8}$ G, in the Local Supercluster. Such high values for the ambient magnetic field in walls and filaments of large scale structure obey observational constraints such as Faraday rotation measurements and seem to be not unrealistic, as recently advertised by Ryu, Kang & Biermann [34]. In this regime, UHE CRs diffuse up to ~ 100 EeV for $B_{\text{rms}} \sim 10^{-7}$ G, and a distance to the source $d \sim 10$ Mpc, and propagate recti-linearly beyond, as first advocated by Wdowczyk & Wolfendale [36]. As a consequence, for sources emitting on timescales large compared to typical propagation times, the spectrum in the diffusive range is steeper than the injection spectrum, and typically scales as $Q(E)E^{-0.6}$, with $Q(E)$ the injection spectrum. This is a result of an interplay between the energy dependent diffusion coefficient and energy loss rates. For sources emitting on smaller timescales, the spectrum tends to be peaked at a certain energy that depends on the turn-on time of the source. Diffusion models present many advantages in the context of UHE CRs. For instance, the switch off of diffusion at high energy might provide a simple way to reconcile the seemingly observed flattening of the UHE CR spectrum above the GZK cut-off with a single power law injection spectrum that is relatively soft, $Q(E) \propto E^{-2.4}$. Moreover, the large deflection angles associated with the strong magnetic fields could explain why no astrophysical counterpart could be associated with the highest energy event, within a $\simeq 2^\circ$ error box.

The problem has been recently reconsidered in Ref. [38], using an analytical solution of the diffusion equation in an infinite medium, matched to the near straight line propagation regime at high energy. Here, we have performed numerical simulations of the full problem, including a plane geometry model of the structure of the local Supercluster, and stochastic pion production energy losses. Our simulations improve on analytical solutions, as they allow to simulate the transition between the diffusive and the non-diffusive regimes, and the non-trivial geometry (here modeled as a planar sheet), with inhomogeneity length scales for the density and magnetic fields of, typically, a few Mpc.

Our results differ from the analytical solutions of diffusion in an infinite medium. As a main effect, we find that the free escape of particles at the boundary, due to the negligible magnetic field outside of the sheet, depletes the low energy diffusive part of the UHE CR spectrum with respect to the high energy (non-diffusive) part. For a distance comparable to the thickness of the sheet, this depletion is a factor $\simeq 5$ as compared to the flux predicted for particles diffusing in an infinite medium (no boundary). We also find that the highly anisotropic geometry of the problem, which is all the more anisotropic when the source distance is smaller or comparable to the largest turbulent eddy, implies a strong relative variation in flux at any energy in the diffusing part, of order 1. Furthermore, our simulations recover the scaling of the diffusion coefficient indicated by analytical estimates, but with about a factor 10 higher normalization both in the infinite medium and for the sheet geometry.

We thus find that, for sources emitting over timescales larger than $\sim 10^8$ yr: (*i*) if the magnetic field is not strong

enough, *i.e.* $B_{\text{rms}} \lesssim 5 \times 10^{-8}$ G, the diffusion coefficient is not small enough to compensate the depletion of low energy diffusive particles by ejection out of the sheet; no entirely satisfying fit to the observed UHE CR spectrum can be obtained in this case. This result holds even for small distances, down to $d \sim 5$ Mpc, as the sheet half-thickness is only ~ 5 Mpc; *(ii)* if the source distance is significantly larger than the thickness of the sheet ~ 10 Mpc, or if source and/or observer are located near the boundary of the sheet, within $\sim \pm 2$ Mpc, there is no consistent fit to the observed UHE CR spectrum. Indeed, in this case, pion production becomes significant and depletes the high energy part of the spectrum, *i.e.* above the GZK cut-off, while the diffusive particles feel quite strongly the presence of the sheet boundary.

However, we find a very nice and consistent fit to the observed UHE CR spectrum for a source distance $d \sim 10$ Mpc, and a magnetic field $B_{\text{rms}} \sim 10^{-7}$ G. Smaller magnetic field strengths suffer from the above problem, while stronger magnetic field imply too much pion production at high energies. Indeed, for the above magnetic field, particles up to ~ 100 EeV diffuse, and diffusion considerably increases the effective distance traveled. We thus obtain a solution only in a limited region of parameter space.

A magnetic field $B_{\text{rms}} \sim 10^{-7}$ G may not be a coincidence after all, as the equipartition field expected in walls of large scale structure, such as the Local Supercluster, is $B_{\text{equi}} \sim 0.3 \mu\text{G} h_{100} (T/3 \times 10^6 \text{ K})^{1/2} (\rho_b/0.3\rho_c)^{1/2}$ [1,34], where T and ρ_b denote respectively the temperature and baryon density within the sheet, while ρ_c is the critical density, and h_{100} the value of the Hubble constant in units of 100 km/s/Mpc.

Based on the technique developed here, we will perform detailed studies of spectra and angular images of ultra-high energy cosmic ray sources for more realistic source and magnetic field distributions in subsequent work.

Next generation experiments with their potential to record tens to hundreds of events above 100 EeV will be able to detect these signatures and exploit the information associated with them.

ACKNOWLEDGMENTS

We especially thank the late David Schramm for constant encouragement and collaboration in earlier work. Pasquale Blasi, Chris Hill, Angela Olinto, and Jörg Rachen are acknowledged for valuable discussions. We are grateful to the Max-Planck Institut für Physik, München (Germany), and the Institut d’Astrophysique de Paris, Paris (France), for providing CPU time. This work was supported, in part, by the DoE, NSF, and NASA at the University of Chicago.

-
- [1] P. P. Kronberg, Rep. Prog. Phys. 57 (1994) 325.
 - [2] G. Sigl, K. Jedamzik, and A. V. Olinto, Phys. Rev. D 55 (1997) 4582.
 - [3] L. Biermann, Zs. Naturforsch. A 5 (1950) 65.
 - [4] J. P. Vallee, Fund. Cosm. Phys. 19 (1997), 1.
 - [5] J. P. Vallee, Astron. Journ. 99 (1990), 459.
 - [6] R. C. Thomson, A. H. Nelson, Month. Not. Roy. Astron. Soc. 201 (1982), 365.
 - [7] J. P. Vallee, J. M. MacLeod, N. W. Broten, Astro. Lett. Communic. 25 (1987), 181.
 - [8] T. A. Enßlin, P. L. Biermann, P. P. Kronberg, and X.-P. Wu, Astrophys. J. 477 (1997) 560.
 - [9] R. M. Kulsrud, R. Cen, J. P. Ostriker, D. Ryu, Astrophys. J. 480 (1997) 481
 - [10] M. A. Lawrence, R. J. O. Reid, and A. A. Watson, J. Phys. G Nucl. Part. Phys. 17 (1991) 733.
 - [11] N. Hayashida et al., Phys. Rev. Lett. 73 (1994) 3491; S. Yoshida et al., Astropart. Phys. 3 (1995) 105; M. Takeda et al., Phys. Rev. Lett. 81 (1998) 1163.
 - [12] N. Hayashida et al., Phys. Rev. Lett 77 (1996) 1000.
 - [13] D. J. Bird et al., Phys. Rev. Lett. 71 (1993) 3401; Astrophys. J. 424 (1994) 491; *ibid.* 441 (1995) 144.
 - [14] K. Greisen, Phys. Rev. Lett. 16 (1966) 748; G. T. Zatsepin and V. A. Kuzmin, Pis’ma Zh. Eksp. Teor. Fiz. 4 (1966) 114 [JETP. Lett. 4 (1966) 78].
 - [15] J. W. Elbert and P. Sommers, Astrophys. J. 441 (1995) 151.
 - [16] F. Halzen, R. A. Vazques, T. Stanev, and H. P. Vankov, Astropart. Phys. 3 (1995) 151.
 - [17] P. L. Biermann, Nucl. Phys. b (Proc. Suppl.) 43 (1995) 221.
 - [18] G. Sigl, D. N. Schramm, and P. Bhattacharjee, Astropart. Phys. 2 (1994) 401.
 - [19] P. L. Biermann and P. A. S. Strittmatter, Astrophys. J. 322 (1987) 643; J. P. Rachen and P. L. Biermann, Astron. Astrophys. 272 (1993) 161; P. L. Biermann, J. Phys. G 23 (1997) 1.
 - [20] E. Waxman, Phys. Rev. Lett. 75 (1995) 386.

- [21] P. Bhattacharjee, C. T. Hill, and D. N. Schramm, Phys. Rev. Lett. 69 (1992) 567.
- [22] G. Sigl, Space. Sci. Rev. 75 (1996) 375.
- [23] T. Stanev et al., Phys. Rev. Lett. 75 (1996) 3056.
- [24] G. Sigl and M. Lemoine, Astropart. Phys. 9 (1998) 65.
- [25] G. Sigl, Proc. of the Workshop: Observing Giant Cosmic Ray Showers for $> 10^{20}$ eV from Space (Univ. Maryland, Nov. 13-15, 1997).
- [26] M. Lemoine, G. Sigl, A. V. Olinto, and D.N. Schramm, Astrophys. J., 486 (1997) L115.
- [27] G. Sigl, D. N. Schramm, S. Lee, P. Coppi, and C. T. Hill, Proc. Natl. Acad. Sci. USA, Vol. 94 (1997) 10501.
- [28] G. Sigl, M. Lemoine, A.V. Olinto, Phys. Rev. D 56 (1997) 4470.
- [29] Proc. of International Symposium on Extremely High Energy Cosmic Rays: Astrophysics and Future Observatories (Institute for Cosmic Ray Research, Tokyo, 1996).
- [30] S. C. Corbató et al., Nucl. Phys. B (Proc. Suppl.) 28B (1992) 36; M. Al-Seady et al., in [29], p. 191.
- [31] M. Teshima et al. Nucl. Phys. B (Proc. Suppl.) 28B (1992) 169; M. Hayashida et al., in [29], p. 205.
- [32] J. W. Cronin, Nucl. Phys. B (Proc. Suppl.) 28B (1992) 213; The Pierre Auger Observatory Design Report (2nd ed.) 14 March 1997.
- [33] J. F. Ormes et al., in Proc. 25th International Cosmic Ray Conference (Durban, 1997), eds.: M. S. Potgieter et al., 5, 273; Y. Takahashi et al., in [29], p. 310.
- [34] D. Ryu, H. Kang, and P. L. Biermann, e-print astro-ph/9803275, to appear in Astron. Astrophys.
- [35] P. L. Biermann, H. Kang, J. P. Rachen, and D. Ryu, e-print astro-ph/9709252, Les Arcs Proc. (1997) p. 227.
- [36] J. Wdowczyk and A. W. Wolfendale, Nature 281 (1979) 356; M. Giler, J. Wdowczyk, and A. W. Wolfendale, J. Phys. G 6 (1980) 1561; V. S. Berezinsky, S. I. Grigor'eva, and V. A. Dogiel, Zh. Eksp. Theor. Fiz. 96 (1989) 798 [Sov. Phys. JETP 69 (1989) 453].
- [37] F. A. Aharonian and J. W. Cronin, Phys. Rev. D 50 (1994) 1892.
- [38] P. Blasi and A. V. Olinto, preprint astro-ph/9806264, submitted to Phys. Rev. D.
- [39] V. S. Berezinsky and S. I. Grigor'eva, Astron. Astrophys. 199 (1988) 1
- [40] S. I. Syrovatskii, Sov. Astron. 3 (1959) 22; see also V. S. Berezinsky, S. V. Bulanov, V. A. Dogiel, V. L. Ginzburg, and V. S. Ptuskin, *Astrophysics of Cosmic Rays* (North-Holland, Amsterdam, 1990).
- [41] G. R. Blumenthal, Phys. Rev. D 1 (1970) 1596.
- [42] T. A. Enßlin, P. L. Biermann, U. Klein, and S. Kohle, Astron. Astrophys. 332 (1998) 395.
- [43] H. Falcke, Gopal-Krishna, P. L. Biermann, Astron. Astrophys. 298 (1995) 395
- [44] J. Bednarz, M. Ostrowski, Phys. Rev. Lett. 80 (1998) 3911

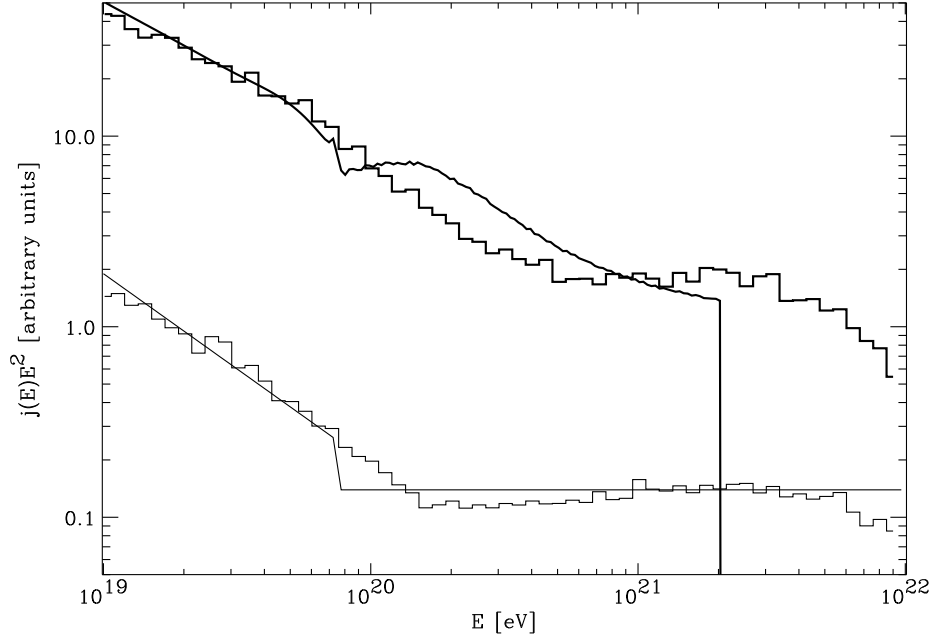


FIG. 1. Spectrum of UHE CRs propagating in an infinite medium, in a turbulent Kolmogorov magnetic field of strength $B_{\text{rms}} \simeq 5 \times 10^{-8}$ G, for a distance to the source $d = 10$ Mpc, a largest turbulent eddy size ~ 10 Mpc, and a numerical cut-off scale $l_c = L/10$. The injection spectrum is $Q(E) \propto E^{-2}$; the spectrum shown is $E^2 j(E)$, with $j(E)$ the observable differential flux, such that the deviation from a horizontal line shows the modification of the injection spectrum. The different cases shown are: no energy loss, in thin solid histogram; energy losses, *i.e.* pair production and stochastic pion production, in thick solid histogram (arbitrarily shifted upwards from the no-energy loss case); analytical approximations to each of the two spectra, obtained from solutions of the equations discussed in the text, in light solid lines (the upper solid line corresponds to the case where energy losses are included, as for the Monte-Carlo results). All fluxes have been normalized to the same total number of 'detected' particles. Analytical and numerical simulations, with energy losses included, differ at high energy $E > 300$ EeV due to the difference between continuous and stochastic energy losses.

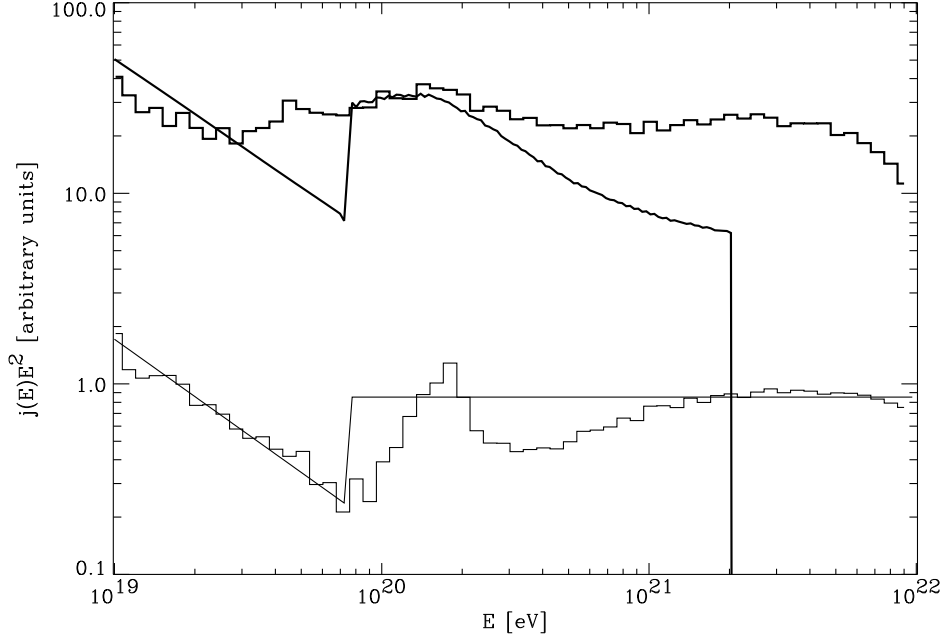


FIG. 2. Same as Fig. 1, except that UHE CRs now propagate in a sheet of finite half-thickness 5 Mpc; both source and observer are located close to the middle-plane.

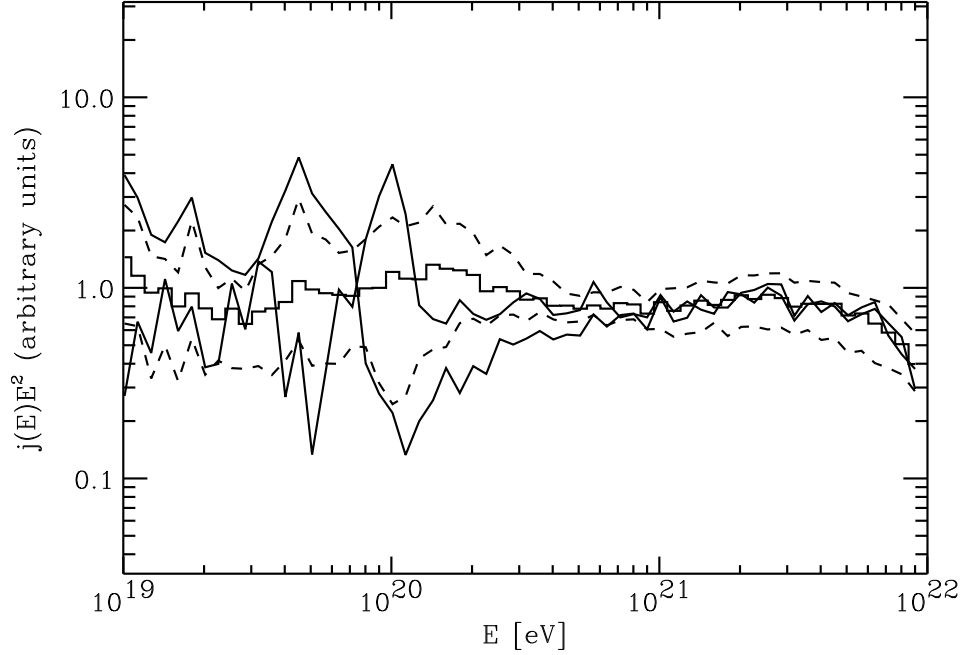


FIG. 3. Spectrum of UHE CRs propagating in a sheet, with the same parameters as in Fig. 2. The solid histogram shows the mean flux, as obtained from the average of 13 fluxes corresponding to different spatial realizations of the magnetic field; the dashed lines show the upper and lower one-sided 1σ deviations from this mean. The light solid lines show two different spectra, corresponding to two different realizations of the magnetic field.

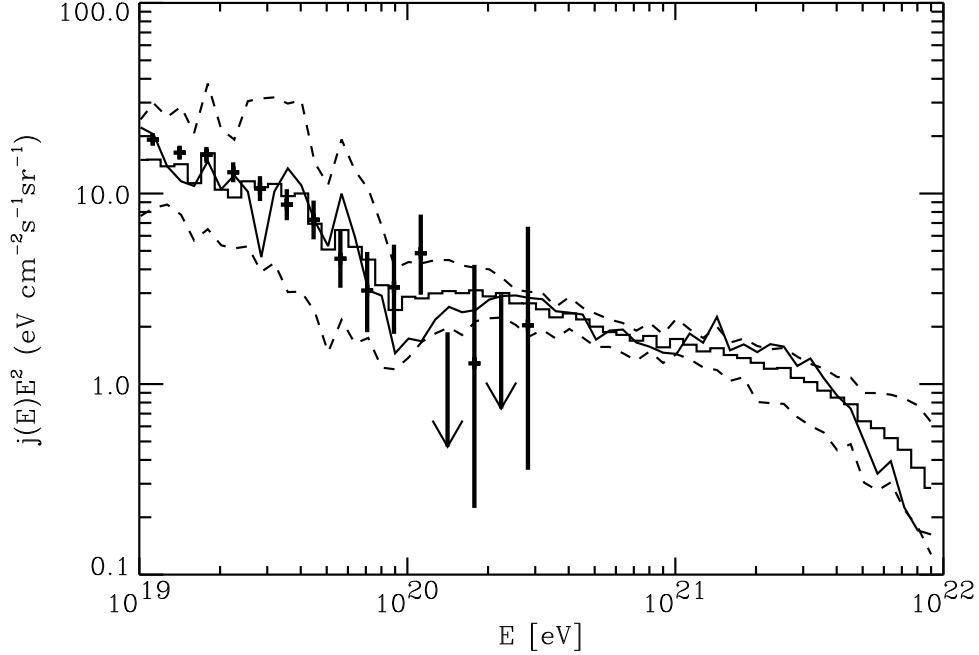


FIG. 4. We show here the best fit obtained, for a magnetic field $B_{\text{rms}} \simeq 5 \times 10^{-8}$ G, a source distance $d = 5$ Mpc, and an injection spectrum $\propto E^{-2.4}$; the data points are obtained from a compilation of the Haverah Park [10], Fly’s Eye [13], and AGASA [11] experiments. The solid histogram shows the mean flux, obtained from the average of 16 different spatial realizations of the turbulent magnetic field, while the light solid line corresponds to one, carefully chosen, best fit, realization of the field.

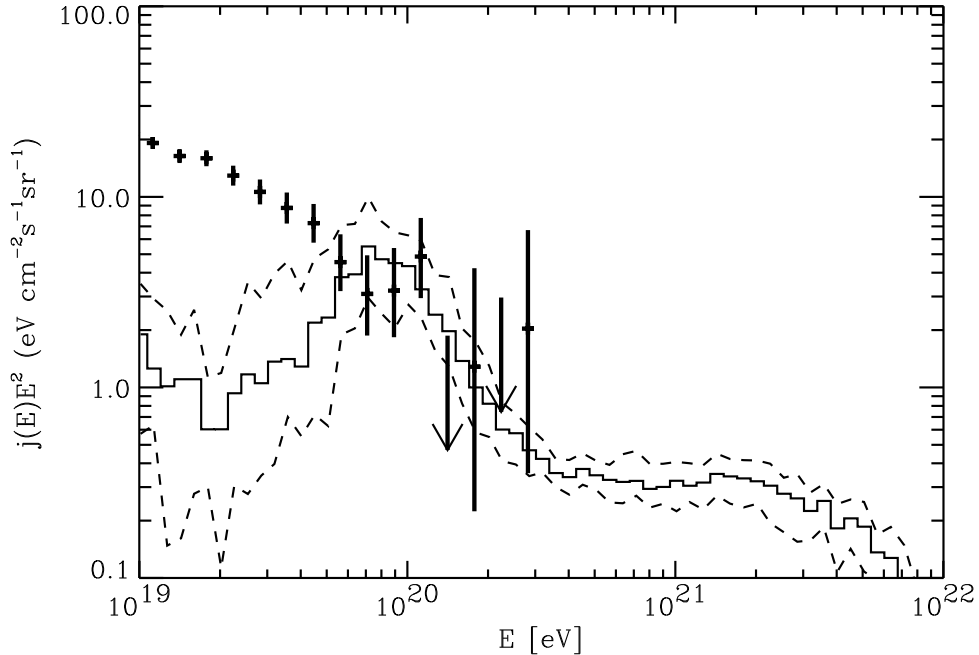


FIG. 5. Spectrum of UHE CRs propagating in the Local Supercluster, for a source distance $d = 25$ Mpc, other physical parameters as in Fig. 4. The solid histogram shows the mean flux, as obtained from the average of fluxes resulting in 11 different spatial realizations of the magnetic field; the dashed lines show the upper and lower one-sided 1σ deviations from this mean.

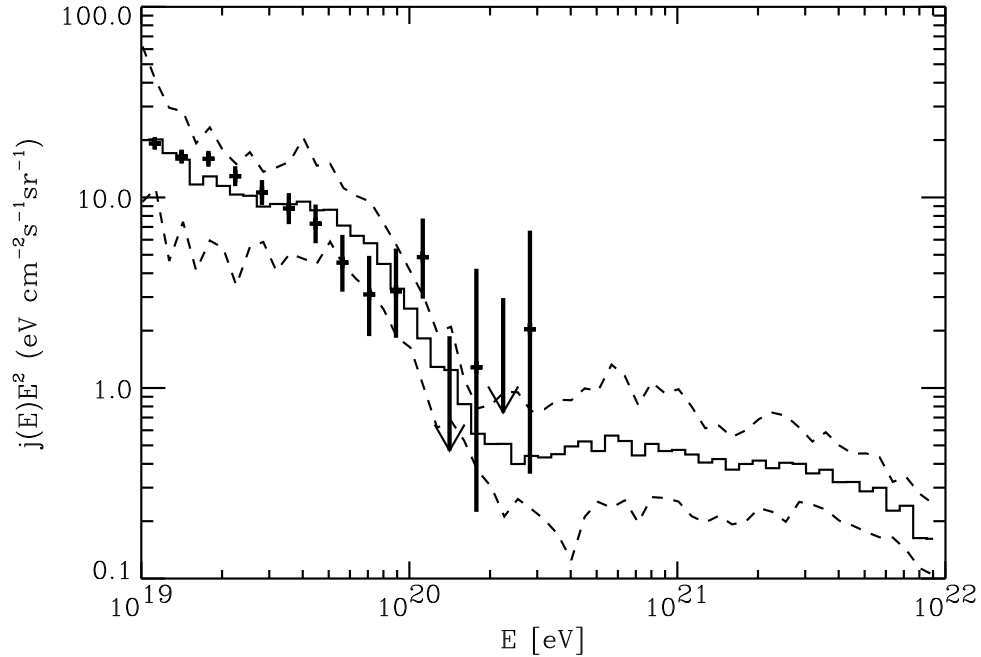


FIG. 6. Spectrum of UHE CRs, as in Fig. 5, but for a source distance $d = 10$ Mpc, and a magnetic field $B_{\text{rms}} \simeq 3 \times 10^{-7}$ G, averaged over 10 field configurations.

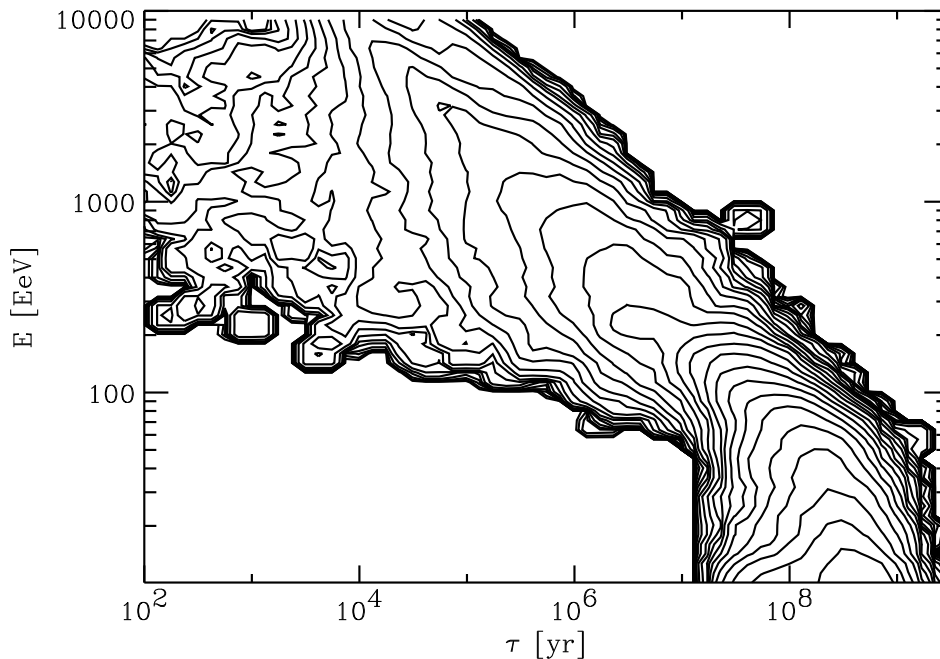


FIG. 7. The distribution of time delays τ_E and energies E for the case shown in Fig. 6. The inter-contour interval is 0.25 in the logarithm to base 10 of the distribution per logarithmic energy and time interval. The three regimes discussed in the text, $\tau_E \propto E^{-2}$ in the rectilinear regime $E \gtrsim 200$ EeV, $\tau_E \propto E^{-1}$ in the Bohm diffusion regime $60 \text{ EeV} \lesssim E \lesssim 200$ EeV, and $\tau_E \propto E^{-1/3}$ for $E \lesssim 60$ EeV are clearly visible.

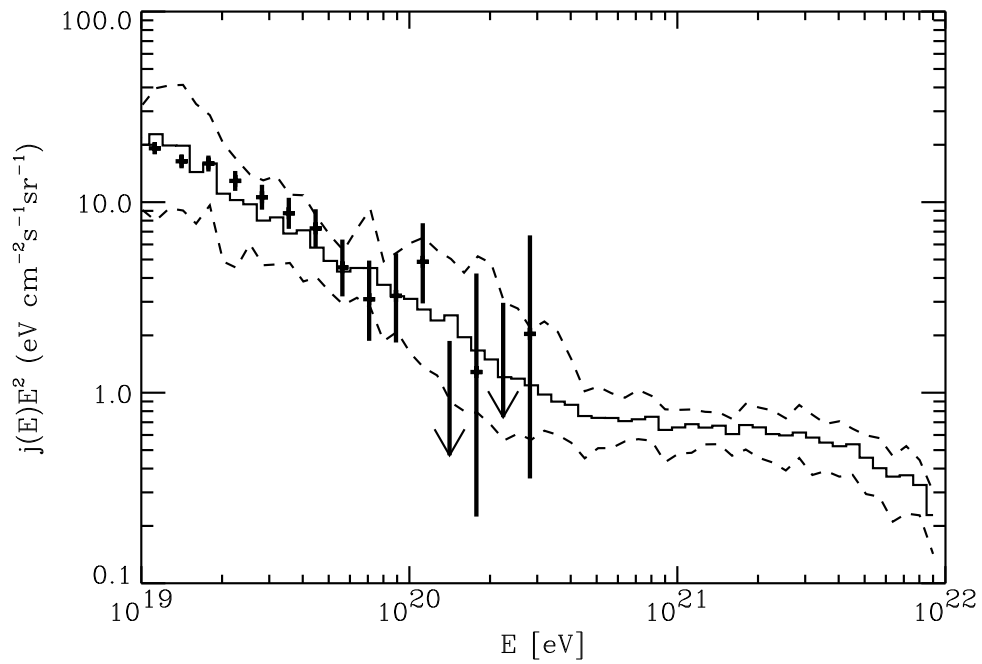


FIG. 8. Final best fit solution, obtained for a source distance $d = 10$ Mpc, and a magnetic field strength $B_{\text{rms}} \simeq 10^{-7}$ G, other physical parameters and line key as in Fig. 5, where the histogram was averaged over 15 field configurations.

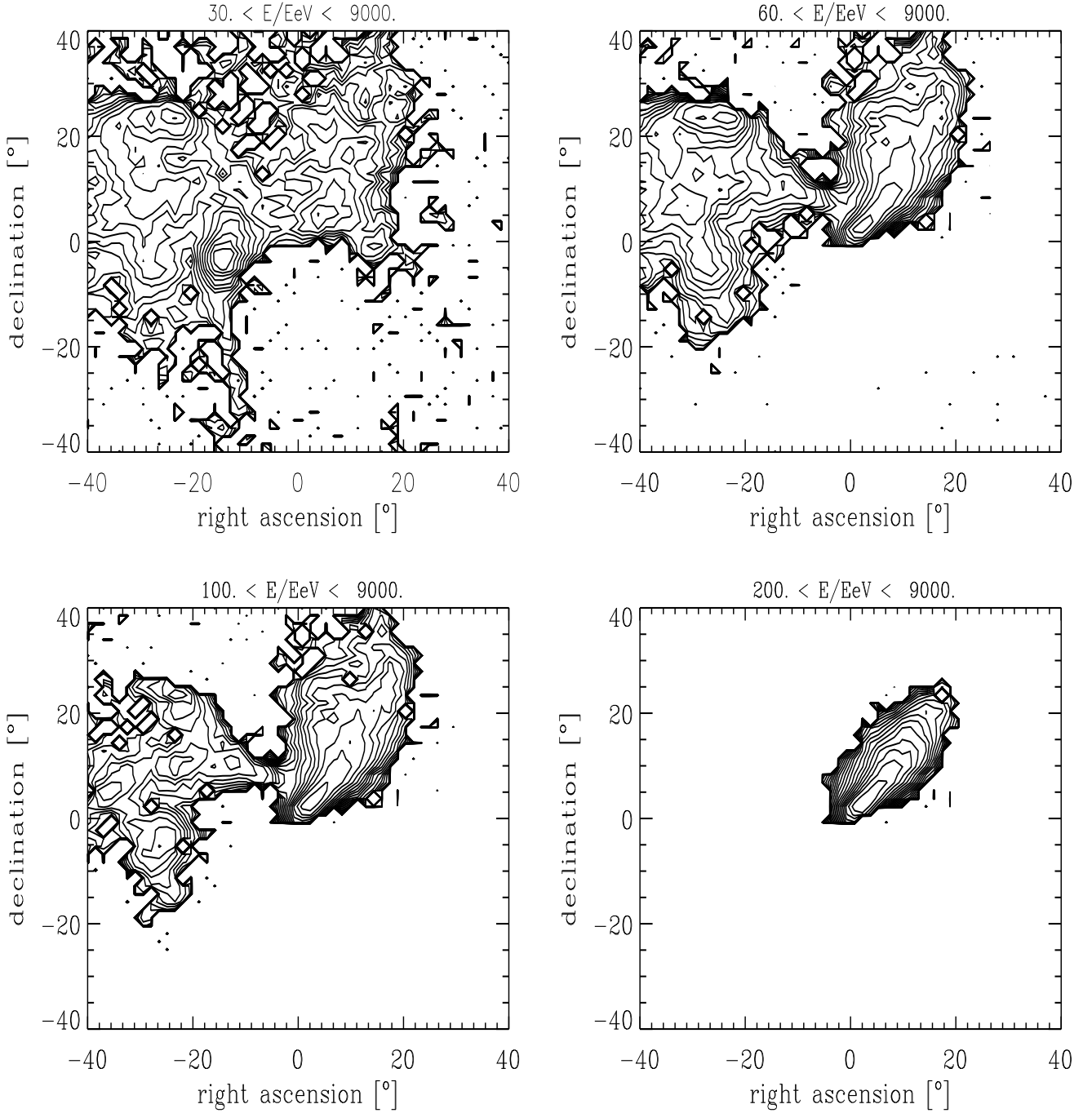


FIG. 9. Angular image of a point-like source, corresponding to one particular realization of the scenario shown in Figs. 2 and 3, as seen by a detector of $\simeq 1^\circ$ angular resolution, in different energy ranges, as indicated. An $E^{-2.4}$ injection spectrum was assumed. A transition from several images at lower energies to only one image at the highest energies occurs where the linear deflection becomes comparable to the effective field coherence length, as discussed in the text. The inter-contour interval is 0.1 in the logarithm to base 10 of the integral flux per solid angle.